chemosensors

MDPI

Article

Pithecellobium dulce Leaf-Derived Carbon Dots for 4-Nitrophenol and Cr(VI) Detection

Simei Darinel Torres Landa [1], Inderbir Kaur [2] and Vivechana Agarwal [1,*]

[1] Center for Research Engineering and Applied Sciences, Autonomous State University of Morelos (CIICAp-UAEM), Av. Univ. 1001, Col. Chamilpa, Cuernavaca 62209, Morelos, Mexico
[2] Department of Electronics, Bhaskaracharya College of Applied Sciences, University of Delhi, Delhi 110075, India
* Correspondence: vagarwal@uaem.mx

Abstract: Luminescent carbon dots (CDs) synthesized from *Pithecellobium dulce* (P. Dulce) leaves, in a simple, single-step carbonization procedure, were used as optical nanosensors. TEM revealed the crystalline nature of the CDs with the average dimension of 20 nm with a quantum yield of 24%. In addition to carbon, the X-ray photoelectron spectroscopy shows the presence of oxygen and nitrogen. The FTIR spectra and Zeta potential were used for additional characterization of the nanoprobes. Among the contaminants and heavy metals, the proposed nanoprobes were found to be selective towards 4-nitrophenol (4-NP) and Cr(VI), respectively. The emission response of CDs towards 4-NP solution not only reveals the high sensitivity of the CDs (Limit of detection (LOD) of 14 nM) but also demonstrates a color change (light to dark yellow) that is attributed to spontaneous deprotonation detectable with the naked eye. The selectivity of CDs towards Cr(VI) (LOD 0.9 nM) was also tested in the presence of other metals. The quenching mechanism has been attributed to the inner filter effect for both analytes. The observed low detection limits in river and tap water opens up the possible applicability of the proposed nanoprobes as optical sensors in environmental pollution monitoring.

Keywords: green synthesis; optical sensor; carbon dots; Cr(VI); 4-Nitrophenol; photoluminescence

Citation: Torres Landa, S.D.; Kaur, I.; Agarwal, V. *Pithecellobium dulce* Leaf-Derived Carbon Dots for 4-Nitrophenol and Cr(VI) Detection. *Chemosensors* **2022**, *10*, 532. https://doi.org/10.3390/chemosensors10120532

Academic Editor: Lin Yuan

Received: 4 October 2022
Accepted: 3 December 2022
Published: 13 December 2022

1. Introduction

With the continual expansion of mankind and the rapid development of industrial technologies, environmental pollution, specifically organic contaminants, heavy metals, bisphenol compounds, and nitroaromatic compounds pollution, has become a serious issue [1,2]. The continuous emission of various manmade chemicals and by-products not only degrades environmental quality but also causes a risk to public health [1]. Nitroaromatic compounds, in particular nitrophenols, are shown to have several uses in the military and chemical industries. The nitrophenol family includes (a) all three isomers of mono-nitrophenols, namely adjacent (2-NP), interphase (3-NP), and antithesis (4-NP/p-NP), and (b) dinitrophenols, namely 2-4 Dinitrophenols (2,4-DNP) and 2,4,6-trinitrophenol (TNP/ picric acid) [3,4]. Unfortunately, all the above mentioned chemicals are also well-known carcinogens. An additional concern is that nitrophenols are difficult to eliminate or degrade from water resources due to their high solubility and stability in water which has the potential to produce more serious environmental issues [5]. As a result of their misuse and uncontrolled disposal, they can cause substantial contamination to the environment, particularly soils, rivers, lakes, and ground water [2]. The p-nitrophenol (4-NP) in particular, is one of the most harmful pollutants created from the production of pesticides, pharmaceuticals, dyes, leather anti-fungal agents, and other industrial goods. As a result of its toxicity and carcinogenicity, the United States Environmental Protection Agency (USEPA) has placed 4-NP on its "Priority Pollutant List". According to the USEPA, the maximum permissible content of 4-NP in drinking water is 0.43 μM [6].

In addition, among the numerous heavy elements, Cr(VI) is one of the most toxic ions, and exposure to it causes cancer along with harm the respiratory system, gastrointestinal system, and immune system [7]. This is due to the extremely soluble nature of Cr(VI) and its massive discharge from various electroplating, tanning, and leather industries, leading to a significant increase in Cr(VI) levels in drinking water. According to EPA guidelines, the maximum contaminant level for total chromium concentrations in drinking water should be less than 100 ppb [7].

On the other hand, traditionally reported 4-NP and Cr(VI) detection strategies, such as electrochemical methods, chromatographic techniques, capillary electrophoresis, and fluorometric assays [6,7] have some limitations, such as the usage of expensive chemicals, time-consuming sample preparation, and extensive analysis times. As a result, developing a cost-effective, simple, and quick approach for accurate determination of the trace amount of 4-NP and Cr(VI) in environmental and drinking water samples is critical. Although semiconductor quantum dots (e.g., CdS, CdTe, CoTe, and SnO_2) have been widely employed for environmental pollution monitoring, their toxicity (due to the use of heavy metal ions) has prompted researchers to look for novel biodegradable and biocompatible nanomaterials [8]. Organic carbon-based quantum dots have attracted attention as a prominent sensing device in the last decade due to their exceptional photochemical stability and photophysical performance. Carbon nanoparticles with a large surface area, enhanced conductivity, and specificity can be used for fast and efficient detection of environmental organic and non-organic toxins [9–11]. The use of toxic chemicals can be minimized even further by synthesizing carbon dots (CDs) with green precursors, which is the preferred technology, with several benefits such as cost-effectiveness and sustainability to organic waste [7,9,12,13].

Several researchers have conducted experiments to detect Cr(VI) selectively. Pineapple juice-derived CDs were used as sensors for Cr(VI) with a linear concentration range (LCR) and an LOD as 0–18 μM and 0.052 μM, respectively [14]. Tulsi leaf-derived CDs (Bhatt et al., 2018) reveal 1.6–50 μM and 0.015 μM as the LCR and LOD, respectively. Many other researchers have used various green sources, such as lemon peel waste [15], groundnuts, and dried rose petals [16] to detect Cr(VI). In addition, apple seeds [3], palm shell powder, and triflic acid (N and S co-doped) [17], and shaddock peel + HCl [18] selectively detected 4-NP with LODs of 13 nM, 79 nM, and 37.1 nM. The reported low LODs for Cr(VI) (i.e., 81 pM [16] and 0.185 nM [19]), using CDs synthesized with dried rose petals and Panax notoginseng, have been achieved through additional nitrogen/sulfur and nitrogen dopants with the green precursors (i.e., ethylenediamine (EDA)/L-cysteine and EDA, respectively).

In this work, we present the one-step synthesis (direct carbonization) of fluorescent CDs with high selectivity towards 4-NP and Cr(VI) under lab conditions as well as in real water samples using only a green and sustainable carbon precursor, *P. Dulce leaves*. Due to the high adaptability to different kinds of soils, Pithecellobium dulce is considered as an abundant and invasive plant in México and other countries. As it has even been declared as a noxious weed in some regions [20] due to which economic and environmental equilibrium may significantly be impacted by these invasive plants, this work presents a way to produce highly functional and versatile material from *Pithecellobium dulce* leaves [20,21].

The proposed fluorescence approach allowed the selective and sensitive detection with a turn-off effect of the nanoprobes in a linear concentration range from 20 to 80 nM with an LOD of 14 nM for 4-NP and an LCR from 10 to 16 nM with an LOD of 0.9 nM for Cr(VI) detection without any additional treatment or incorporation of dopant to the as-prepared CDs.

2. Materials and Methods

2.1. Materials

P. Dulce leaves were collected from the local streets of Cuernavaca City, Morelos State, Mexico (18.954602, −99.220129). 4-nitrophenol (4-NP, 99.5%) was procured from Sigma Aldrich. Except where the use of tap or river water is specified, all the general

studies utilized deionized water. Phenol, 4-aminophenol, 2-aminophenol, and catechol were acquired from Sigma Aldrich. Metal salts were acquired from Fermont, including potassium dichromate -K_2CrO_7 (99%), coper sulfate -$CuSO_4$, cobalt sulphate -$CoSO_4$ (99%), nickel sulfate -$NiSO_4$ (98%), ferrous sulfate (II) -$FeSO_4$ (99%), cadmium nitrate -$Cd(NO_3)_2$ (99%), -$Mg(NO_3)_2$ (99.5%), silver nitrate -$AgNO_3$ (99%), barium nitrate -$Ba(NO_3)_2$ (99%), zinc chloride -$ZnCl_2$ (97.2%), ferric chloride (III) -$FeCl_3$ (97%), ferrous chloride (II) -$FeCl_2$ (98%), tin chloride -$SnCl_2$ (99%), lead chloride -$PbCl_2$ (99%), copper chloride -$CuCl_2$ (99%), cobalt chloride -$CoCl_2$ (98%), and mercury chloride -$HgCl_2$ (99.5%).

2.2. Methods

P. Dulce leaves were washed and dried in a dehydrator at 40 °C for 4 h. The dried carbon precursor was ground in a coffee mill for 30 s. Carbon dots were synthesized by direct carbonization in a muffle furnace at 200 °C for 120 min. The TGA analysis for leaves at 200 °C revealed a mass loss of 9.9 % (Figure S1). The generated carbonaceous material was utilized to make solutions with a concentration of 10 mg/mL that were treated in an ultrasonic bath for 4 h before being centrifuged at 13,000 revolutions for 20 min. Following this, filtering was performed using 2 μm filter paper. The filtrate was refrigerated in order to preserve the CDs to be used for further studies. The estimated concentration is 1.4 mg/mL for final stock solution. The quantum yield (QY) was calculated with rhodamine 6G in water (QY_x = 92% [22]) as a reference, using the equation:

$$QY_x = QY_{st}\left(\frac{K_x}{K_{st}}\right)\left(\frac{\eta_x}{\eta_{st}}\right)^2 \quad (1)$$

where K is the slope from the linear regression of integrated luminescence vs. the absorbance of st and x (subscripts) for the standard and sample, respectively. The refractive index of the aq. solution is taken as η = 1.33 for both low-concentration solutions. Absorbance values were kept less than 0.1 to achieve the linear relationship of absorbance at different molar concentrations [23] of the CDs as well as the reference.

A UV–Vis (Perkin Elmer Lambda 900) spectrophotometer and fluorescence (Varian Cary Eclipse) spectrometer were used to investigate the optical properties of synthesized CDs. The primary functional groups that are present in the ground leaf samples were evaluated using FT-IR (Varian Cary Eclipse) to see how their presence or composition changed after the pyrolithic carbonization temperature treatment. To determine the particle size distribution of the synthesized CDs, high-resolution transmission electron microscopy (HR-TEM) measurements were performed through TEM-JEOL JEM-2010. For surface sensitive quantitative analysis, a Thermo Scientific scalab 250Xi X-ray photoelectron spectrometer (XPS) was used. The ZP (zeta potential) measurements were performed using a Malvern zeta sizer. A Rigaku X-ray diffractometer (XRD) was employed for measuring the diffraction pattern using monochromatized Cu Kα radiation (λ = 1.54 Å).

3. Results

3.1. Characterization of CDs

The existence of a maxima at 325 nm and 260 nm in the absorbance spectra (Figure 1a) is attributed to n to π* and π to π* transitions with carbon–carbon and carbon–oxygen molecular unsaturated centers, respectively. Although CDs appear to be pale yellow in daylight, under UV light, a blue emission was observed (inset Figure 1a) indicating the high fluorescence emission. CDs showed an intense peak corresponding to emission at 428 nm after optimal excitation at 325 nm. The estimated QY of the as-synthesized CDs was 24% (Figure S2) considering the slope of the integrated signal corresponding to fluorescence intensity vs. absorbance for CDs and Rhodamine 6G as a reference. On the other hand, the main functional groups found on the raw leaves before and after carbonization were identified through Fourier transform infrared spectroscopy, as depicted in Figure 1b. Vibrational bands were observed at 3606 cm^{-1} with a medium sharp -OH stretching; the band located at 2915 cm^{-1} refers to the C-H group [24,25], while the peak

at 1693 cm^{-1} is generated by the C=O strength [24], at 1528 cm^{-1}, the band of medium binding of N-H corresponds to the scissor vibration of NH_2, and at 1415 cm^{-1}, a vibration band of C-OH was detected [26]. The C-O strength signal appears at 1047 cm^{-1} [27], and the peak at 880 cm^{-1} is attributed to the C-H functional group [28].

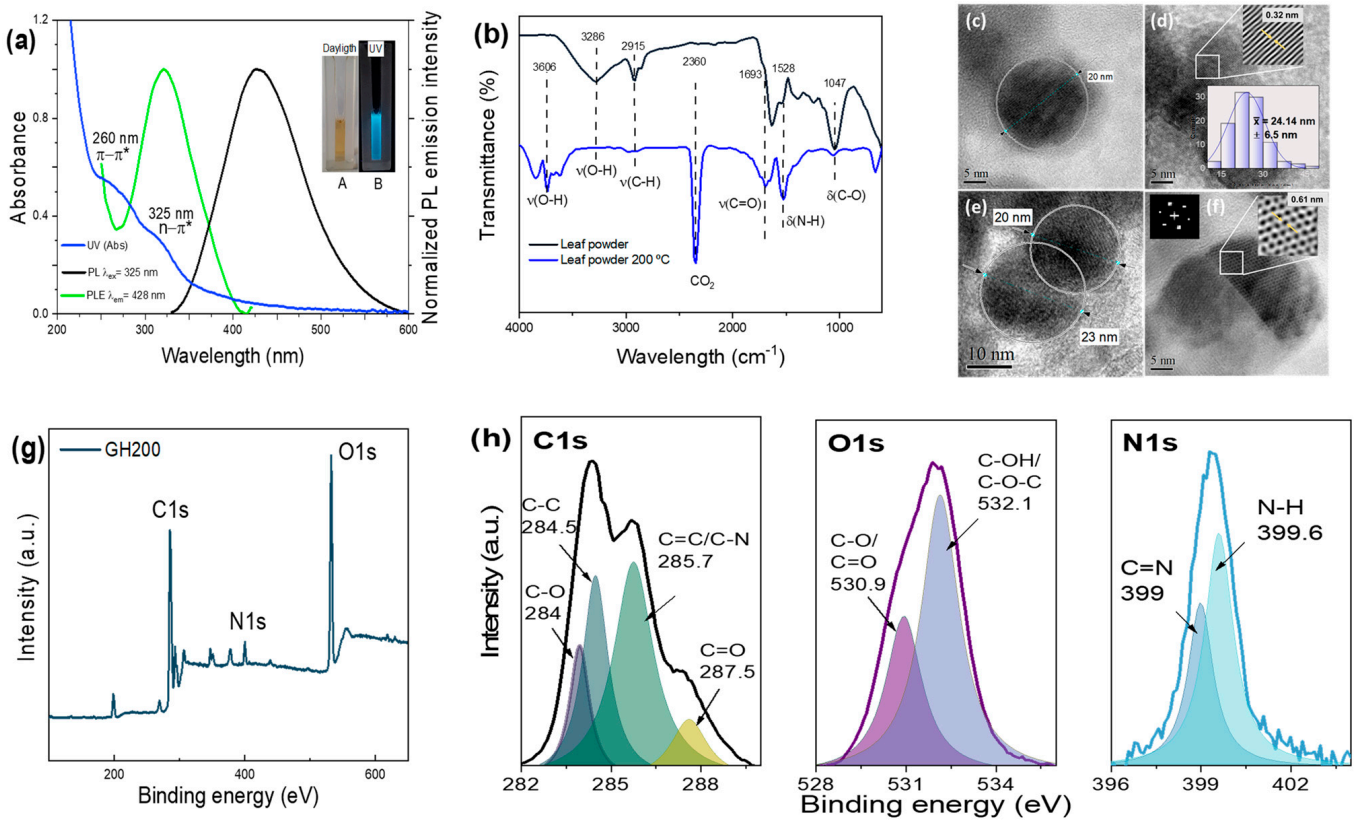

Figure 1. (**a**) Absorbance, photoluminescence (PL) emission, and photoluminescence excitation (PLE) spectra of the synthesized CDs (inset: photographic image of the CDs suspended in water, under daylight (A) and UV light (B)), (**b**) FTIR spectra of raw and carbonized leaves, (**c**–**f**) TEM micrographs (inset in (**d**) reveal the magnified view of interplanar distance and the particle size distribution), (**g**) XPS survey, and (**h**) high-resolution XPS spectra corresponding to C1s, O1s, and N1s of CDs.

The TEM images reveal a spherical morphology (Figure 1c–f). The size distribution of the as-prepared CDs revealed a particle size range of 10–50 nm (average diameter: 24.14 ± 6.5 nm; the histogram is taken over 100 particles shown as an inset in Figure 1d with the crystal lattice spacing of 0.32 nm (inset in Figure 1d). The chemical composition of the CDs was confirmed with XPS experiments, where the results revealed the presence of C, O, and a weak signal for N (survey scan in Figure 1g) on the surface of the carbon dots. The calculated atomic percentages majorly show the presence of carbon and oxygen (~65 and 35%) and a slight presence of nitrogen (Figure S3). The high-resolution deconvoluted XPS spectrum of the carbonized sample, Figure 1h, reveals the C1s spectra with four bands located at 284, 284.5, 285.7, and 287.5 eV, corresponding to C-O, C-C, C-N/C=N, and C=O [29–32] in the C 1s spectrum of carbon dots, respectively. Two signals are observed in the high-resolution O 1s spectrum at 530.9 eV (C-O/C=O are present) and at about 532.1 eV, corresponding to C-OH/C-O-C bonds [33,34]. In addition, CDs showed a weak signal in the N1s spectrum with two peaks around 399 and 399.6 eV attributed to groups C=N and N-H [35]. As per Clogston et al.[36], the Z-potential near to ±10 mV (close to be neutral) could tend to form agglomerates. In the present case, the Z-potential value of −12 mV supports the anionic character of carbonized particles.

3.2. Selectivity of CDs for 4-Nitrophenol and Chromium (VI)

To assess the selectivity of CDs, the changes in the fluorescence intensity in the presence of different organic pollutants were measured. The fluorescence response of CDs for 4 NP was more sensitive than that of other organic phenolic compounds. A complete PL quenching (turn-off) was observed in the presence of 4 NP (Figure 2a,b). While assessing the selectivity towards different metals, it is important to consider that the most common ions found in rivers and lakes around the world are Al, As, Cd, Co, Cr, Cu, Fe, Hg, Mn, Ni, Pb, and Zn [37]. The majority of these ions along with others such as Ba, Hg, and Mg were tested to observe the analytical performance of the proposed nanoprobes towards the heavy metals present in the water.

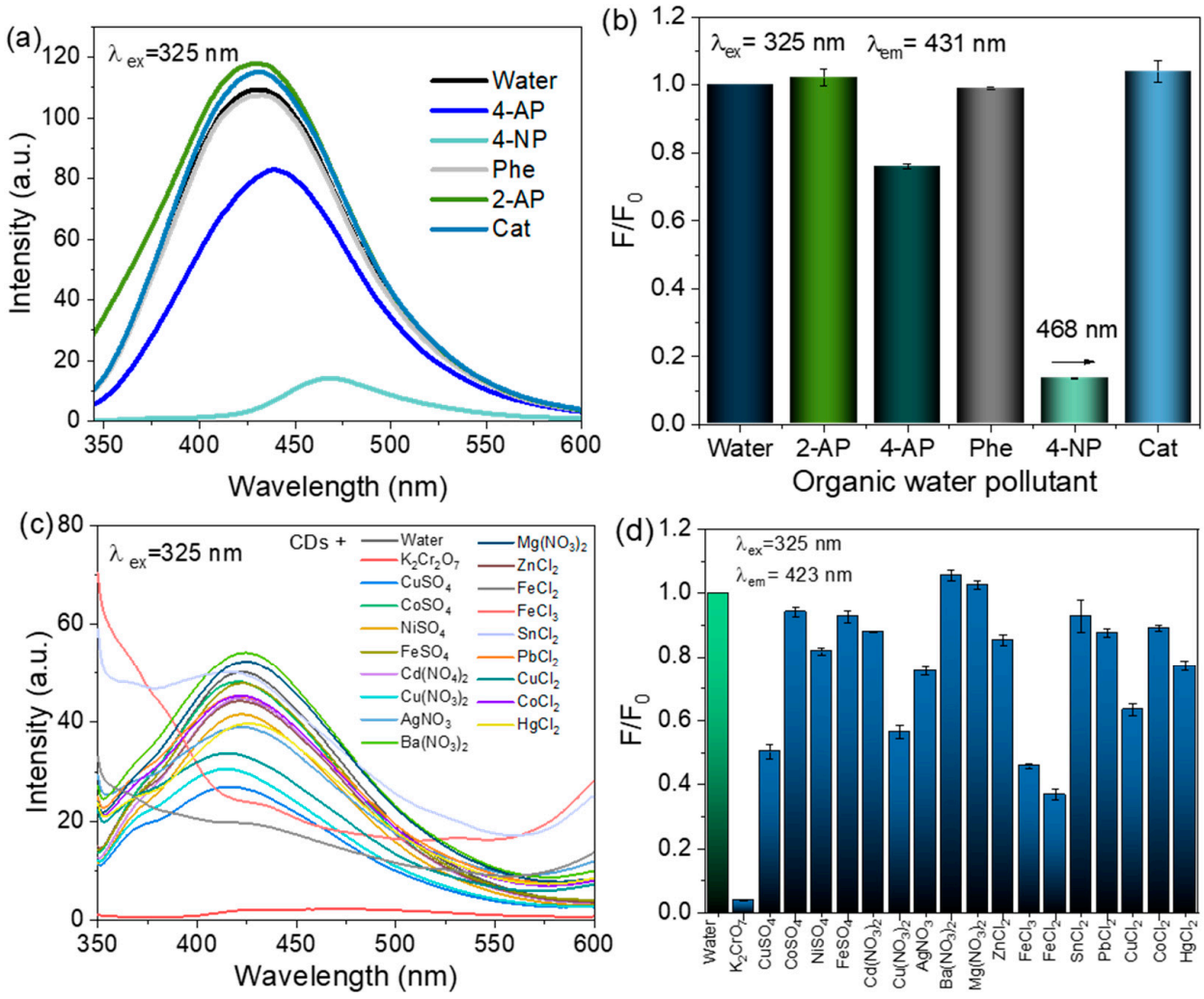

Figure 2. Selectivity studies of CDs towards different organic pollutants in deionized water: (**a**) PL emission spectra taken at a 1 mM concentration of the analyte, (volumetric ratio of analytes,: CDs: total volume 1:120) and (**b**) relative/normalized PL peak emission intensity (F/F_0) (with respect to the control) for each analyte, where F0 is the control, i.e., PL is the peak intensity of only CDs; and (**c**) PL response towards different metal ions taken at 10 mM of metal ion concentration and (**d**) relative/normalized PL peak emission intensity (F/F_0) (with respect to the control) for each metal ion.

The optical signal of the CDs in the presence of different metal ions, was found to quench selectively for Cr(VI) (Figure 2c,d). In addition, in low and high concentrations of 4-NP and Cr(VI) analytes, a significant displacement of the maximum PL peak occurs.

3.3. Sensitivity Assessment for 4-Nitrophenol Using P. dulce-Derived CDs

Figure 3a includes the sensitivity experiment of CDs towards 4-NP from 20 nm to 2 mM LCR of 4-NP in DI water with a PL turn-off effect, along with a spectral redshift (maximum wavelength signal shifted by 30 nm).

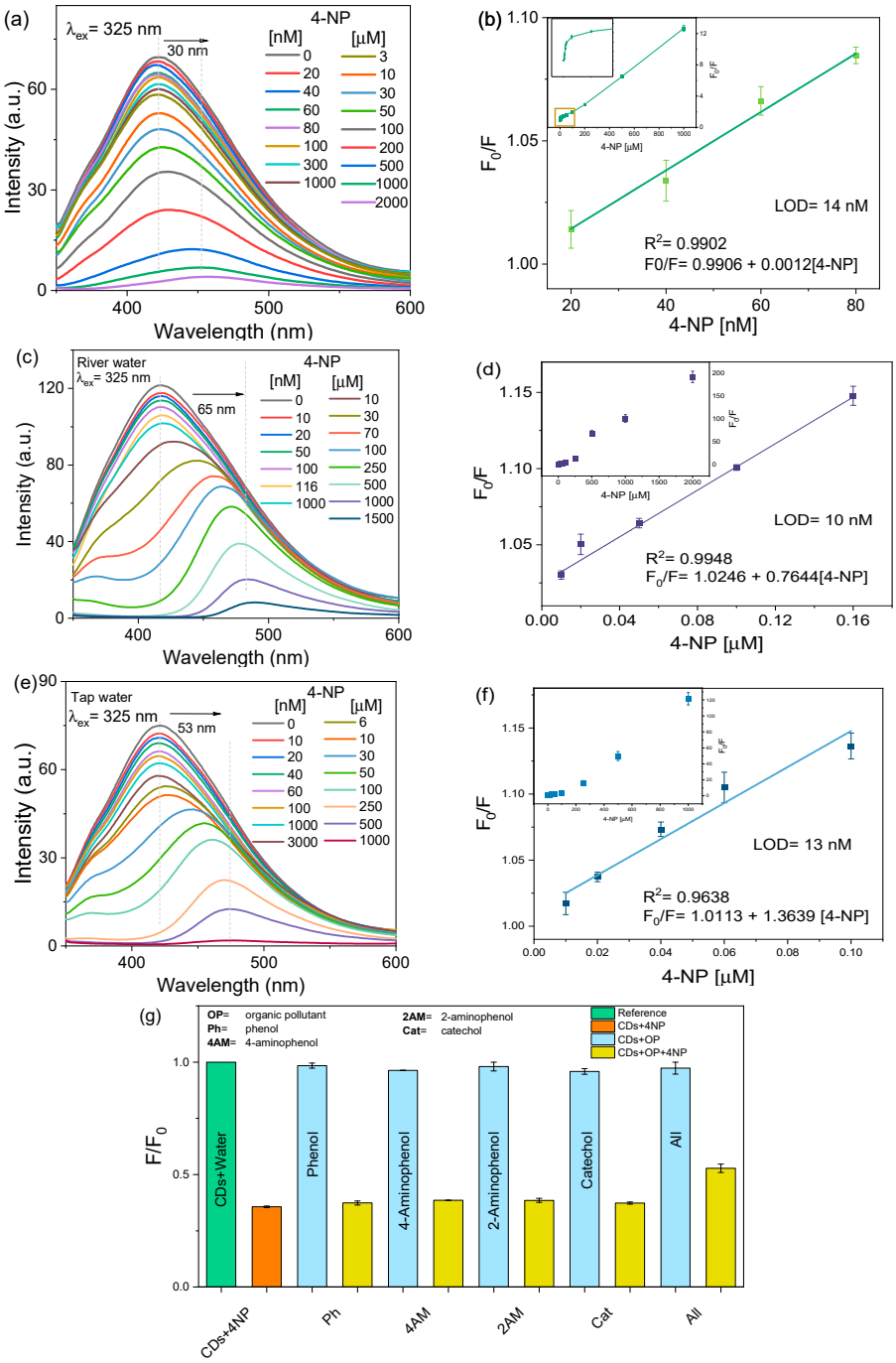

Figure 3. (**a**) Sensitivity of CDs towards different concentration of 4-NP in deionized water and (**b**) Stern–Volmer fit for estimating the LOD of F_0/F vs. 4-NP, where F_0 is the fluorescence intensity of CDs in water (control) and F is the intensity of CDs + 4-NP from 20 nM to 2 mM. (**c**) Sensitivity of CDs towards different concentrations of 4-NP in river water, (**d**) F_0/F vs. 4-NP concentration; Stern-Volmer fit for estimating LOD, (**e**) Sensitivity of CDs towards different concentration of 4-NP in tap water, (**f**) Stern–Volmer adjustment and LOD for 4-NP in tap water, and (**g**) interference test in detection of 4-NP (deionized water).

Figure 3b represents the Stern–Volmer equation ($F_0/F = 0.9906 + 0.0012$ [4-NP]) with an R^2 of 0.9902 and an estimated LOD of 14 nM in the linear range of 20 to 80 nM. The Stern–Volmer relation is defined by $F_0/F = 1 + K_{SV}$ [Q], where K_{SV} is the slope and Q is the analyte concentration. The LOD is estimated according to $3\sigma/S$, where σ is the standard deviation of the response of the the carbon solution signal without the analyte and S is the slope of the calibration plot in a good linear fitting range [38,39]. The results of the evaluation of 4-NP sensitivity in river water from 10 µM to 1.5 mM with a bathochromic shift of 65 nm and fitted data in linear adjustment from 10 to 160 nM are shown in Figure 3c and its corresponding figure (Figure 3d) uses a Stern–Volmer equation ($F_0/F = 1.026 + 0.7644$ [4-NP], $R^2 = 0.9948$) with an estimated LOD of 10 nM. The evaluation of 4-NP in tap water is depicted in Figure 3e with an LCR of 10 nm–1 mM and a Stern Volmer equation of $F_0/F = 1.0113 + 1.3639$ [4-NP], $R^2 = 0.9638$ and a red shift of 53 nm (Figure 3f). The LOD was observed as 13 nM in the concentration linear range between 10 to 100 nM. A comparison of F_0/F vs. different concentrations of 4-NP in deionized, river, and tap water is included in Figure S4a.

3.4. Interference Studies for 4-NP

Various organic pollutants were tested in deionized water for their ability to quench the PL of the CDs as potential interfering contaminants' in the 4-NP detection. For interference studies, 100 µM of 4-NP and 100 µM of other contaminants solutions were prepared. The resulting data allow us to conclude that potential interferences have no impact on the feasibility in 4-NP optical sensing (Figure 3g).

However, compared to the PL intensity corresponding to each tested organic pollutant, the presence of 4-NP decreased the possible observation of the quenching signal, when all the tested organic pollutants were present.

3.5. Sensitivity Assessment for Chromium (VI)

As shown in Figure 4a, sensitivity experiments using nanoprobes that were also selective for Cr(VI) were performed in the range 3 nM to 2.5 mM; the maximum emission peak was maintained at 420 nm with low-concentration solutions, i.e., from 3 nM to 7 µM, however, the PL band is then slightly redshifted. Figure 4b shows the corresponding Stern–Volmer equation ($F_0/F = 0.7563 + 0.0314$ [4-NP]) with the R^2 of 0.9986 and an estimated LOD of 0.9 nM. The Cr(VI) in river water was tested in the range of 20 nM to 2 mM (Figure 4c). The obtained Stern–Volmer equation was $F_0/F = 0.9882 + 1.0414$ [Cr(VI)] with the R^2 of 0.9907 and an estimated LOD of 7 nM is depicted in Figure 4d. In the case of detection for Cr(VI) in tap water (Figure 4e), there is a low concentration range (from 10 nM to 10 µM) in which the maximum PL peak is steady around 423 nm, while in higher concentrations (100 µM to 2 mM), a displacement of the signal is observed (around 50 nm). The Stern–Volmer equation for tap water is $F_0/F = 1.0255 + 2.0607$[Cr(VI)] with an R^2 of 0.9883 and LOD of 8 nM (Figure 4f). A comparison of F_0/F vs. different concentrations of Cr(VI) in deionized, river, and tap water is included in Figure S4b indicating a high proximity in the large range of 3 nM to 1000 µM.

The LODs of CDs from the proposed *P. Dulce* were compared with the values of other carbon dots obtained from other different leaves to detect 4-NP and chromium (VI) (Ref. to Table S1 [5,40] and Table S2 [7,41,42]).

The difference in the S-V constants between deionized, river, and tap water is due to the difference in their properties, such as the conductivity and pH that can possibly contribute to the different linear concentration range. The measured conductivities (mS/cm) for deionized water, tap water, and river water are 0.0061, 0.1103, and 1.12, respectively. On the other hand, the pH values of deionized water, tap water, and river water are 5.69, 7.65, and 7.5, respectively.

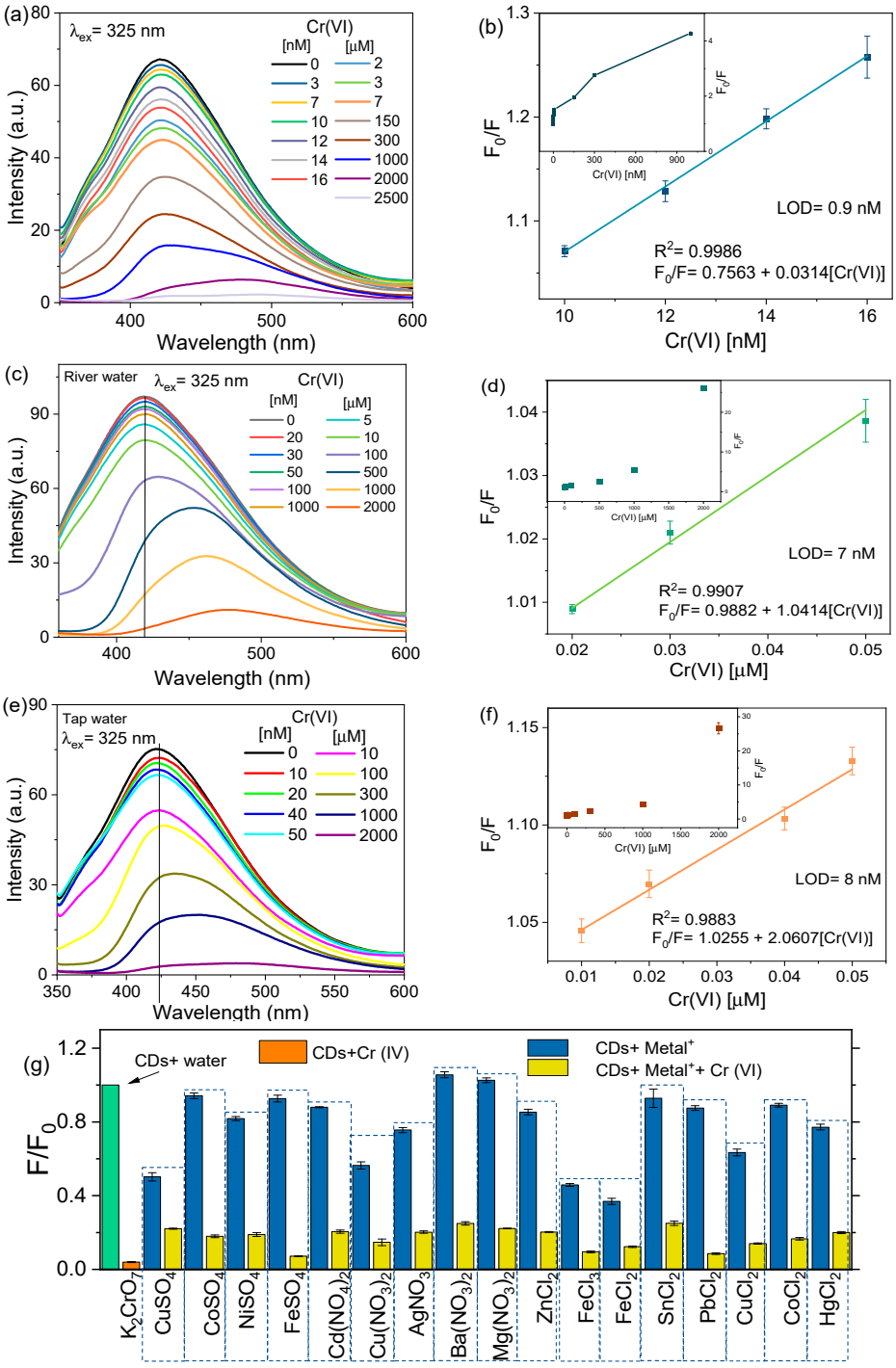

Figure 4. Sensitivity of CDs towards different concentrations of Cr(VI) in (**a**) DI water, (**b**) river water, and (**c**) tap water. Stern–Volmer fit, F_0/F vs. 4-NP concentration for LOD calculation (**d**) in the range of 10 to 160 nM in DI water and (**e**) in the range of 20 to 50 nM in river water, (**f**) in tap water (10–50 nM), and (**g**) interference studies of metal ions vs. Cr(VI) detection.

After a certain range, the relationship between concentration of the analyte and photoluminescence signal is not well correlated, which has been attributed to the differences in the interaction between the CDs and the analyte molecule [43], i.e., when the analyte concentration is increased, due to the limited number of CDs, the mutual interaction between analyte–CDs is reduced and the distance between the CDs and quencher is modified, as can be corroborated in the red shift of PL bands (in accordance with [44]). The

aforementioned behavior has been reported previously in numerous works, for example, Tammina and Yang [45], reported the influence of 4-NP concentration (0.25–125 µM) on the emission intensity of N-CDs; nevertheless, they observed a linear graph between F/Fo vs. the concentration of 4-NP in the low range of 0.25–7.5 µM, with an LOD of 50 nM when using 10 µL of N-CDs. After this range, the detection of this analyte could not be controlled with the same accuracy. The same restriction in the range of detection was observed in the detection of Cr(VI). On the other hand, Singh et al. obtained carbon dots from Dunaliella salina biomass to detect Cr(VI) and they observed a narrow linear range from 30 to 180 nm with a good correlation coefficient with an LOD of 18 nM from the tested range of 0.04–25 µM [46]. Similarly, Pooja D. et al. used *Carica papaya* waste pulp to obtain CDs for total chromium detection in the range of 10 ppb to 1000 ppm. No continuous correlation between PL intensity and analyte concentration was observed; nevertheless, the detection was possible in the LCR of 10–100 ppb with an LOD of 0.708 ppb with R^2 of 96.74 [47]. Nevertheless, when the CD concentration is increased, the LODs and the linear ranges can be also increased and detect the analytes with considerable accuracy in higher concentrations, as has been demonstrated in other works from our research group [48]. In addition, although low concentrations of nanoprobes (CDs) can quantify a huge range of analyte concentrations, there can possibly be more than one slope for acquiring a linear optical signal with respect to the analyte concentration (present case). Hence, the possibility of varying the CD concentration, for different predefined ranges of analyte, should be considered.

3.6. Interference Studies for Cr(VI) Detection

PL quenching in the presence of Cr(VI) was assessed and compared with other metal ions. Mixtures of 100 µM of Cr(VI) and 100 µM of the aforementioned pollutant metal ions were used. The difference of Cr(VI) in a one-to-one concentration with other metal ions confirms negligible interference when these metal ions are present individually with Cr(VI) (Figure 4g).

3.7. Effect of Temperature, pH, and Salinity

Apart from the abovementioned analysis, some additional measurements were conducted, such as the effect of salinity, temperature, and pH on the optical response of the nanoprobes. A decrease/increase in PL intensity with an increase/decrease in temperature reveals a reversible cycling behavior from 25 to 70 °C. (Figure S5a–c). The obtained data were linearly fitted with an $R^2 = 0.96$. The influence of the concentration of chlorides on the emission intensity was analyzed with the help of optical measurements at different concentrations of NaCl. CDs show a stable emission signal in chlorides in the tested concentration range of 0.5 to 4 M (Figure S5d). The proposed nanoprobes show a stable response at diverse pH values with the exception of extreme values of 1 and 14 where the photoluminescence intensity diminishes. There is currently no definite consensus among researchers on how to explain the influence of pH on the luminescence response of CDs [49].

3.8. Possible Mechanism of PL Quenching for 4-NP and Cr(VI)

There are different sensing mechanisms proposed for fluorescent particles. CDs in environmental monitoring mainly include the dynamic/static quenching effect, Förster resonance energy transfer (FRET), inner filter effect (IFE), photoinduced electron transfer (PET), and surface energy transfer (SET). In particular, the IFE consists of the absorption of both the excitation and emission wavelengths or only signals emitted by the absorbers [13,38,50] as was observed in the corresponding sensing nanoprobe systems (in this case, 4NP and Cr(VI)). The absorption spectrum of 4-NP (ref. to Figure 5a) centered at 315 nm overlaps with the excitation spectrum of the CDs at ~260–390 nm. On the other hand, Cr(VI) possess three absorbance bands (260, 360, and 440 nm; ref to Figure S6) and an overlap among the emission band at 325 and the PL band of CDs (428 nm) with the absorbance bands of Cr(VI) supporting the turn-off mechanism due to the IFE [50–52].

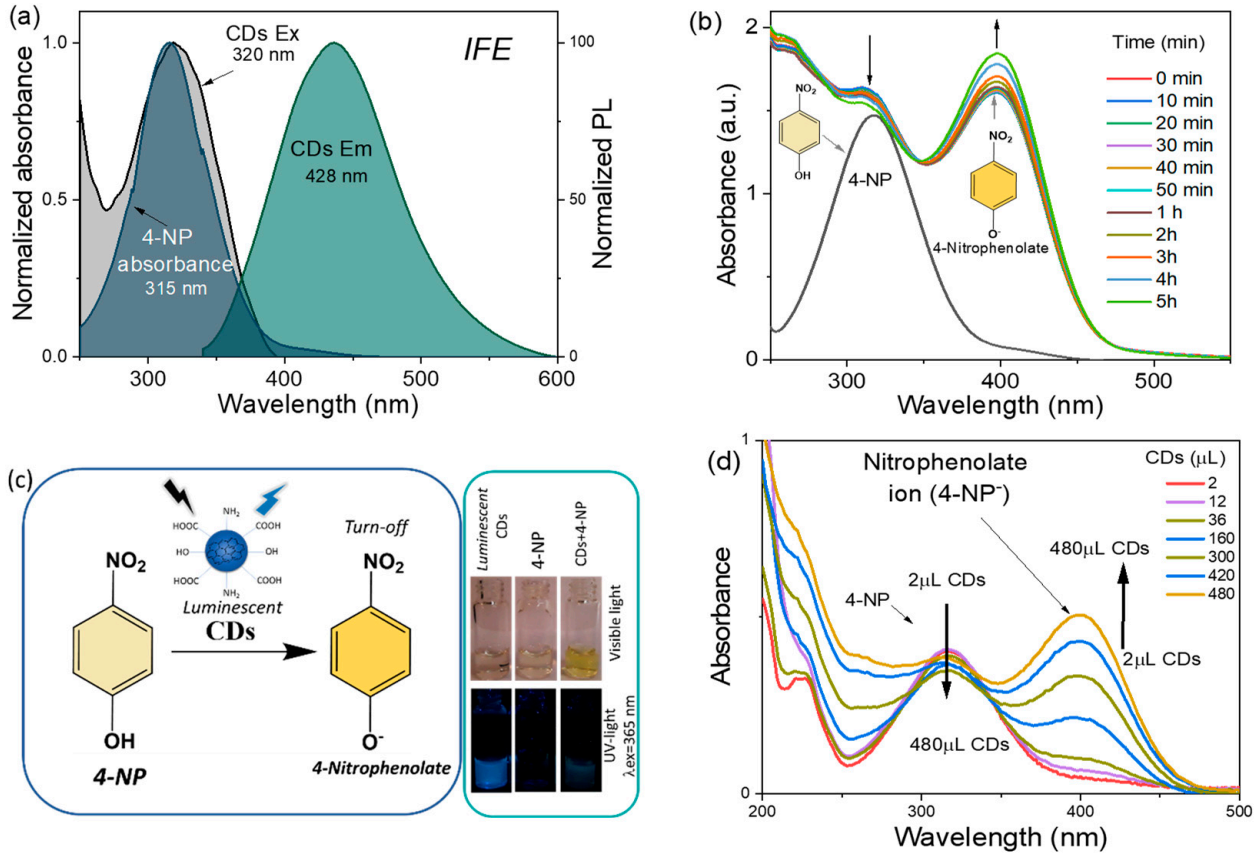

Figure 5. (**a**) Inner filter effect projected as a possible mechanism of 4-NP sensing/deprotonation, (**b**) changes in 4-NP + CDs absorbance at different times, (**c**) schematic representation of possible mechanism of PL quenching and images showing the change of color in visible light and under UV light, and (**d**) evolution of 4-nitrophenolate ion peak at different concentrations of CDs at initial time.

Moreover, a redshift in the PL signal (when either the 4-NP or Cr(VI) concentration is increased) was observed. According to Zhang et al., the emission peak shift in PL bands of CDs, in the presence of high concentrations of Cr(VI) ions, may be attributed to the coordination interaction of the Cr(VI) and functional groups containing nitrogen (of CDs), i.e., imidazole groups attached to the CDs' surface [44].

On the other hand, Xiao et al. observed a red-shift in the maximum of the emission band of their co-doped CDs when the 4-NP concentration was increased and concluded that the shift was a consequence of the IFE [53]. Similarly, Qin et. al. attributed the selective detection of 4-NP (using CDs from Escherichia coli) to the IFE mechanism which was accompanied by the red-shifted emission peak [54]. Tummala et al. suggested that the red-shift in fluorescence is also related to the deprotonation of 4-NP to a 4-nitrophenolate ion with IFE as the possible quenching mechanism [55].

Additionally, Wang et al. related this phenomenon to the quantum effect and the distribution of emissive traps on the surface of the nitrogen and silicon co-doped CDs [56]. El-Shaheny et al. detected o- and p-nitrophenols with graphene quantum dots. Based on the corresponding suppressed efficiency (%E), they determined that the fluorescence quenching by both nitrophenols originates from IFE. This conclusion was supported by the gradual red shift of the fluorescence maxima at high quencher concentrations [57].

The PL maximum band of *P. Dulce* CDs was noticeably red shifted for 4-NP (30, 65, and 53 nm for deionized, river, and tap water at a concentration of 1 mM of 4-NP) and for Cr(VI) (32, 44, and 14 for deionized, river, and tap water at a concentration of 1 mM of Cr(VI)) as possible evidence of the predominant IFE mechanism. In addition, with the help

of diphenyl carbazide (DPC) assay (Figure S8) the possibility of partial reduction of Cr(VI) to Cr(III) can also be considered [58]. Further studies are needed to confirm the possibility.

In addition, the UV absorption wavelength of 4-NP was red shifted from 315 nm to 400 nm, Figure 5b) in the presence of the CDs. The absorbance intensity was increased with the increase in the interaction time, due to the formation of a 4-nitrophenolate ion. The red shift is related to the deprotonation of 4-NP to a 4-nitrophenolate ion and the same phenomenon was reflected in the change of color from transparent to yellow [59] (Figure 5c).

The noticeable change in color is accompanied by a minor decrease in the band intensity corresponding to 4 -nitrophenol (band at 320nm (in absorbance); Figure 5d not only gives an additional confirmation of the change of 4-NP concentration but also opens up a possibility for their usage as dual-sensors (absorbance and PL). The luminescence quenching and the formation of the 4-nitrophenolate ion is possibly induced by the functional groups around the CDs' surface. The pH for the CDs' stock solution was approximately ~7 whereas the pH value for 4-NP was obtained around 5. The pH rises to almost 6.9 when CDs interact with the phenolic solution to generate the deprotonation of 4-NP to 4-nitrophenolate ion. The pH increment has been reported in other deprotonation stages from 4-NP to 4-NP ion, when sodium borohydride has been used as a reducing agent [60].

3.9. Interference Studies for 4-NP and Cr(VI) with Respect to Each Other

A couple of experiments were performed to study the interference between the contaminant 4-NP and Cr(VI) (Figure S7), with the fixed concentration of either 4-NP or Cr(VI) (100 μM) and changing concentration of another analyte Cr(VI)/4-NP in the concentration range of 0.5 to 500 μM. Although the presence of either of the contaminant (4-NP/Cr(VI)) solution is not found to interfere with the detection of the other analyte (Cr(VI)/4-NP), the addition of the 4-NP in the Cr(VI) solution reveals a relatively predominant F/F_0 ratio response.

4. Conclusions

A simple green synthesis (carbonization at 200 °C) of blue light emitting carbon dots from *Pithecellobium dulce* leaves was demonstrated. The absorbance bands maximum at 260 and 325 nm have been attributed to n-π* and π-π* transitions with C-C from the core and C-O molecular unsaturated centers from the surface, respectively. The relative quantum yield was determined to be 24% using Rhodamine 6G as a reference. The CDs' size of approx. 20 nm and interplanar spacing of 0.32 nm were estimated by TEM. The XPS signal corresponding to carbon, confirms the presence of C-O, C-C, C=C/C-N, and C=O. The oxygen spectrum discloses the presence of C-O/C=O, C-OH / C-O-C groups, and nitrogen 1s reveals C=N and N-H functionalized surface. The optical response of the CDs remains stable/invariable under different pH (2–13) and saline solutions. The nanoprobes were found to be selective towards 4-NP and Cr(VI) with very low limits of detection in deionized water, i.e., 14 and 0.9 nM, respectively. The efficacy of the CDs for 4-NP has been demonstrated in river and tap water with similar LODs of 10 and 13 nM, respectively. Similarly, for Cr(VI), apart from the low LODs of 7 and 8 nM in river and tap water, respectively. Apart from producing an added value product from the abundant biowaste (*P. Dulce*), the proposed CDs show a lower LOD than other CDs from leaves based biomass, without adding any additional dopants. A simultaneous decrease in the absorbance band of 4-NP at ~320 nm and the emergence of a 4-nitrophenolate ion band that increased proportionally with CDs' concentration indicated the deprotonation of 4NP in addition to an incremental change in pH. Apart from the formation of the 4-nitrophenolate ion, the luminescence quenching in the presence of 4-NP has been attributed to an inner filter effect, which also dominates in Cr(VI) detection. The deprotonation of 4-NP using *P. Dulce* can be further investigated for possible catalytic applications. The suggested simple, one-step, cost-effective synthesis method and detection technique make the proposed nanoprobes a possible strong option for the construction of sensitive optical sensors for 4-NP and Cr(VI) in environmental applications.

Supplementary Materials: The following supporting information can be downloaded at: https://www.mdpi.com/article/10.3390/chemosensors10120532/s1, Figure S1: TGA of raw carbon precursor analysis; Figure S2: (a) Fluorescence integral intensity vs. absorbance for the quantum yield calculation. Rhodamine 6G was used as a reference; Figure S3: Elemental percentage calculated from XPS; Figure S4: Comparison of F0/F vs. different concentrations of (a) 4-NP and (b) Cr(VI) in deionized, river, and tap water; Figure S5: Stability studies. PL emission of CDs as a function of (a–c) temperature, (d) different concentrations of saline solution, and (e) pH; Figure S6: Cr(VI) absorbance bands; PL emission and PL excitation spectra of CDs; Figure S7: Interference between fixed concentration of 4-NP (125 μM) with different concentrations of Cr(VI) and fixed concentrations of Cr(VI) (125 μM) with different concentrations of 4-NP; Figure S8: Absorbance relationship C/C0 for determination of residual Cr (VI) at 540 nm wavelength by indirect colorimetric method with diphenyl carbazide (DPC) assay; Table S1: Detection of 4-NP using CDs derived from leaves; Table S2: Detection of Cr(VI) using CDs derived from leaves.

Author Contributions: Conceptualization, S.D.T.L. and V.A.; methodology S.D.T.L. and V.A.; formal analysis S.D.T.L. and I.K.; investigation S.D.T.L. and V.A.; writing—original draft preparation, S.D.T.L. and I.K.; writing—review and editing, S.D.T.L., I.K. and V.A.; visualization, V.A.; supervision V.A.; project administration V.A.; funding acquisition V.A. All authors have read and agreed to the published version of the manuscript.

Funding: This research was funded by CONACyT Basic Sciences project Ref.- A1-S-30393.

Institutional Review Board Statement: Not applicable.

Informed Consent Statement: Not applicable.

Data Availability Statement: Not applicable.

Acknowledgments: V.A. acknowledges support from CONACyT, ST-CVU 624330, and is thankful to CONACyT for the scholarship provided.

Conflicts of Interest: The authors declare no conflict of interest.

References

1. Tu, Y.; Wang, S.; Yuan, X.; Wei, Y.; Qin, K.; Zhang, Q.; Chen, X.; Ji, X. A novel fluorescent nitrogen, phosphorus-doped carbon dots derived from Ganoderma Lucidum for bioimaging and high selective two nitrophenols detection. *Dye. Pigment.* **2020**, *178*, 108316. [CrossRef]
2. Wan, Y.; Wang, M.; Zhang, K.; Fu, Q.; Gao, M.; Wang, L.; Xia, Z.; Gao, D. Facile and green synthesis of fluorescent carbon dots from the flowers of *Abelmoschus manihot* (Linn.) Medicus for sensitive detection of 2,4,6-trinitrophenol and cellular imaging. *Microchem. J.* **2019**, *148*, 385–396. [CrossRef]
3. Chatzimarkou, A.; Chatzimitakos, T.G.; Kasouni, A.; Sygellou, L.; Avgeropoulos, A.; Stalikas, C.D. Selective FRET-based sensing of 4-nitrophenol and cell imaging capitalizing on the fluorescent properties of carbon nanodots from apple seeds. *Sens. Actuators B Chem.* **2018**, *258*, 1152–1160. [CrossRef]
4. Zhang, Q.; Liang, J.; Zhao, L.; Wang, Y.; Zheng, Y.; Wu, Y.; Jiang, L. Synthesis of Novel Fluorescent Carbon Quantum Dots From Rosa roxburghii for Rapid and Highly Selective Detection of o-nitrophenol and Cellular Imaging. *Front. Chem.* **2020**, *8*, 665. [CrossRef] [PubMed]
5. Qu, Y.; Yu, L.; Zhu, B.; Chai, F.; Su, Z. Green synthesis of carbon dots by celery leaves for use as fluorescent paper sensors for the detection of nitrophenols. *New J. Chem.* **2020**, *44*, 1500–1507. [CrossRef]
6. Hu, Y.; Gao, Z. Sewage sludge in microwave oven: A sustainable synthetic approach toward carbon dots for fluorescent sensing of para-Nitrophenol. *J. Hazard. Mater.* **2020**, *382*, 121048. [CrossRef]
7. Bhatt, S.; Bhatt, M.; Kumar, A.; Vyas, G.; Gajaria, T.; Paul, P. Green route for synthesis of multifunctional fluorescent carbon dots from Tulsi leaves and its application as Cr(VI) sensors, bio-imaging and patterning agents. *Colloids Surf. B Biointerfaces* **2018**, *167*, 126–133. [CrossRef]
8. Pedrero, M.; Campuzano, S.; Pingarrón, J. Quantum Dots as Components of Electrochemical Sensing Platforms for the Detection of Environmental and Food Pollutants: A Review. *J. AOAC Int.* **2017**, *100*, 950–961. [CrossRef]
9. Landa, S.D.T.; Bogireddy, N.K.R.; Kaur, I.; Batra, V.; Agarwal, V. Heavy metal ion detection using green precursor derived carbon dots. *iScience* **2022**, *25*, 103816. [CrossRef]
10. Ajith, M.P.; Pardhiya, S.; Rajamani, P. Carbon Dots: An Excellent Fluorescent Probe for Contaminant Sensing and Remediation. *Small* **2022**, *18*, 2105579. [CrossRef]
11. Kaur, I.; Batra, V.; Bogireddy, N.K.R.; Landa, S.D.T.; Agarwal, V. Detection of organic pollutants, food additives and antibiotics using sustainable carbon dots. *Food Chem.* **2022**, *406*, 135029. [CrossRef] [PubMed]

12. Han, Y.; Yang, W.; Luo, X.; He, X.; Zhao, H.; Tang, W.; Yue, T.; Li, Z. Carbon dots based ratiometric fluorescent sensing platform for food safety. *Crit. Rev. Food Sci. Nutr.* **2022**, *62*, 244–260. [CrossRef] [PubMed]
13. Tu, Y.; Wang, S.; Yuan, X.; Song, P.; Wei, Y.; Qin, K.; Zhang, Q.; Ji, X. Hydrothermal synthesis of *Auricularia auricula* derived nitrogen, phosphorus-doped carbon dots and application in Ag(i) and 4-nitrophenol detection and bioimaging. *Anal. Methods* **2020**, *12*, 2237–2243. [CrossRef]
14. Sharma, S.; Umar, A.; Mehta, S.K.; Kansal, S.K. Fluorescent spongy carbon nanoglobules derived from pineapple juice: A potential sensing probe for specific and selective detection of chromium (VI) ions. *Ceram. Int.* **2017**, *43*, 7011–7019. [CrossRef]
15. Tyagi, A.; Tripathi, K.M.; Singh, N.; Choudhary, S.; Gupta, R.K. Green synthesis of carbon quantum dots from lemon peel waste: Applications in sensing and photocatalysis. *RSC Adv.* **2016**, *6*, 72423–72432. [CrossRef]
16. Das, M.; Thakkar, H.; Patel, D.; Thakore, S. Repurposing the domestic organic waste into green emissive carbon dots and carbonized adsorbent: A sustainable zero waste process for metal sensing and dye sequestration. *J. Environ. Chem. Eng.* **2021**, *9*, 106312. [CrossRef]
17. Soni, H.; Pamidimukkala, P.S. Green synthesis of N, S co-doped carbon quantum dots from triflic acid treated palm shell waste and their application in nitrophenol sensing. *Mater. Res. Bull.* **2018**, *108*, 250–254. [CrossRef]
18. Wang, H.; Zhang, L.; Guo, X.; Dong, W.; Shuang, S.; Gong, X.; Dong, C. Comparative study of Cl,N-Cdots and N-Cdots and application for trinitrophenol and ClO− sensor and cell-imaging. *Anal. Chim. Acta* **2019**, *1091*, 76–87. [CrossRef]
19. Zheng, X.; Qin, K.; He, L.; Ding, Y.; Luo, Q.; Zhang, C.; Cui, X.; Tan, Y.; Li, L.; Wei, Y. Novel fluorescent nitrogen-doped carbon dots derived from *Panax notoginseng* for bioimaging and high selectivity detection of Cr^{6+}. *Analyst* **2021**, *146*, 911–919. [CrossRef]
20. CAB International. "Invasive Species Compendium," CAB International, Datasheet. 2019. Available online: https://www.cabi.org/isc/datasheet/41187#tosummaryOfInvasiveness (accessed on 30 November 2022).
21. Pullaiah, T.; Ielmini, M.R. (Eds.) *Invasive Alien Species: Observations and Issues from around the World*, 1st ed.; Wiley: Oxford, UK, 2021. [CrossRef]
22. Brouwer, A.M. Standards for photoluminescence quantum yield measurements in solution (IUPAC Technical Report). *Pure Appl. Chem.* **2011**, *83*, 2213–2228. [CrossRef]
23. Lin, H.; Huang, J.; Ding, L. Preparation of Carbon Dots with High-Fluorescence Quantum Yield and Their Application in Dopamine Fluorescence Probe and Cellular Imaging. *J. Nanomater.* **2019**, *2019*, 5037243. [CrossRef]
24. Kurdekar, A.; Chunduri, L.A.A.; Bulagonda, E.P.; Haleyurgirisetty, M.K.; Kamisetti, V.; Hewlett, I.K. Comparative performance evaluation of carbon dot-based paper immunoassay on Whatman filter paper and nitrocellulose paper in the detection of HIV infection. *Microfluid. Nanofluidics* **2016**, *20*, 99. [CrossRef]
25. Thakur, M.; Pandey, S.; Mewada, A.; Patil, V.; Khade, M.; Goshi, E.; Sharon, M. Antibiotic Conjugated Fluorescent Carbon Dots as a Theranostic Agent for Controlled Drug Release, Bioimaging, and Enhanced Antimicrobial Activity. *J. Drug Deliv.* **2014**, *2014*, 9. [CrossRef] [PubMed]
26. Kondratenko, T.; Ovchinnikov, O.; Grevtseva, I.; Smirnov, M.; Erina, O.; Khokhlov, V.; Darinsky, B.; Tatianina, E. Thioglycolic Acid FTIR Spectra on Ag2S Quantum Dots Interfaces. *Materials* **2020**, *13*, 909. [CrossRef] [PubMed]
27. Başoğlu, A.; Ocak, Ü.; Gümrükçüoğlu, A. Synthesis of Microwave-Assisted Fluorescence Carbon Quantum Dots Using Roasted–Chickpeas and its Applications for Sensitive and Selective Detection of Fe3+ Ions. *J. Fluoresc.* **2020**, *30*, 515–526. [CrossRef] [PubMed]
28. Li, Y.; Zhong, X.; Rider, A.E.; Furman, S.A.; Ostrikov, K. Fast, energy-efficient synthesis of luminescent carbon quantum dots. *Green Chem.* **2014**, *16*, 2566–2570. [CrossRef]
29. Gao, N.; Huang, L.; Li, T.; Song, J.; Hu, H.; Liu, Y.; Ramakrishna, S. Application of carbon dots in dye-sensitized solar cells: A review. *J. Appl. Polym. Sci.* **2020**, *137*, 48443. [CrossRef]
30. Kehrer, M.; Duchoslav, J.; Hinterreiter, A.; Cobet, M.; Mehic, A.; Stehrer, T.; Stifter, D. XPS investigation on the reactivity of surface imine groups with TFAA. *Plasma Process. Polym.* **2019**, *16*, 1800160. [CrossRef]
31. Jia, L.; Chen, R.; Xu, J.; Zhang, L.; Chen, X.; Bi, N.; Gou, J.; Zhao, T. A stick-like intelligent multicolor nano-sensor for the detection of tetracycline: The integration of nano-clay and carbon dots. *J. Hazard. Mater.* **2021**, *413*, 125296. [CrossRef]
32. Zhu, J.; Chu, H.; Wang, T.; Wang, C.; Wei, Y. Fluorescent probe based nitrogen doped carbon quantum dots with solid-state fluorescence for the detection of Hg2+ and Fe3+ in aqueous solution. *Microchem. J.* **2020**, *158*, 105142. [CrossRef]
33. Jin, X.; Sun, X.; Chen, G.; Ding, L.; Li, Y.; Liu, Z.; Wang, Z.; Pan, W.; Hu, C.; Wang, J. pH-sensitive carbon dots for the visualization of regulation of intracellular pH inside living pathogenic fungal cells. *Carbon* **2015**, *81*, 388–395. [CrossRef]
34. Rezaei, A.; Hadian-Dehkordi, L.; Samadian, H.; Jaymand, M.; Targhan, H.; Ramazani, A.; Adibi, H.; Deng, X.; Zheng, L.; Zheng, H. Pseudohomogeneous metallic catalyst based on tungstate-decorated amphiphilic carbon quantum dots for selective oxidative scission of alkenes to aldehyde. *Sci. Rep.* **2021**, *11*, 4411. [CrossRef]
35. Han, L.; Liu, S.G.; Dong, J.X.; Liang, J.Y.; Li, L.J.; Li, N.B.; Luo, H.Q. Facile synthesis of multicolor photoluminescent polymer carbon dots with surface-state energy gap-controlled emission. *J. Mater. Chem. C* **2017**, *5*, 10785–10793. [CrossRef]
36. Clogston, J.D.; Patri, A.K. Zeta potential measurement. In *Characterization of Nanoparticles Intended for Drug Delivery*; McNeil, S.E., Ed.; Humana Press: Totowa, NJ, USA, 2011; Volume 697, pp. 63–70.
37. Zhou, Q.; Yang, N.; Li, Y.; Ren, B.; Ding, X.; Bian, H.; Yao, X. Total concentrations and sources of heavy metal pollution in global river and lake water bodies from 1972 to 2017. *Glob. Ecol. Conserv.* **2020**, *22*, e00925. [CrossRef]

38. Bu, L.; Peng, J.; Peng, H.; Liu, S.; Xiao, H.; Liu, D.; Pan, Z.; Chen, Y.; Chen, F.; He, Y. Fluorescent carbon dots for the sensitive detection of Cr(vi) in aqueous media and their application in test papers. *RSC Adv.* **2016**, *6*, 95469–95475. [CrossRef]
39. Dhenadhayalan, N.; Lin, K.-C. Chemically Induced Fluorescence Switching of Carbon-Dots and Its Multiple Logic Gate Implementation. *Sci. Rep.* **2015**, *5*, 10012. [CrossRef]
40. Wang, C.; Xu, J.; Zhang, R.; Zhao, W. Facile and low-energy-consumption synthesis of dual-functional carbon dots from Cornus walteri leaves for detection of p-nitrophenol and photocatalytic degradation of dyes. *Colloids Surf. Physicochem. Eng. Asp.* **2022**, *640*, 128351. [CrossRef]
41. Garg, A.K.; Kaushik, J.; Saini, D.; Aggarwal, R.; Sonkar, S.K. Doped Carbon Dots for the Selective Sensing of Hexavalent Chromium in Water. *J. Inst. Eng. India Ser. E* **2022**, *103*, 157–165. [CrossRef]
42. John, B.K.; John, N.; Mathew, S.; Korah, B.K.; Punnoose, M.S.; Mathew, B. Fluorescent carbon quantum dots as a novel solution and paper strip-based dual sensor for the selective detection of Cr(VI) ions. *Diam. Relat. Mater.* **2022**, *126*, 109138. [CrossRef]
43. Herbani, Y.; Suliyanti, M.M. Concentration effect on optical properties of carbon dots at room temperature. *J. Lumin* **2018**, *198*, 215–219. [CrossRef]
44. Zhang, S.; Jin, L.; Liu, J.; Wang, Q.; Jiao, L. A label-free yellow-emissive carbon dot-based nanosensor for sensitive and selective ratiometric detection of chromium (VI) in environmental water samples. *Mater. Chem. Phys.* **2020**, *248*, 122912. [CrossRef]
45. Tammina, S.K.; Yang, Y. Highly sensitive and selective detection of 4-nitrophenol, and on-off-on fluorescence sensor for Cr (VI) and ascorbic acid detection by glucosamine derived n-doped carbon dots. *J. Photochem. Photobiol. A Chem.* **2020**, *387*, 112134. [CrossRef]
46. Singh, A.K.; Singh, V.K.; Singh, M.; Singh, P.; Khadim, S.R.; Singh, U.; Koch, B.; Hasan, S.; Asthana, R. One pot hydrothermal synthesis of fluorescent NP-carbon dots derived from Dunaliella salina biomass and its application in on-off sensing of Hg (II), Cr (VI) and live cell imaging. *J. Photochem. Photobiol. A Chem.* **2019**, *376*, 63–72. [CrossRef]
47. Pooja, D.; Singh, L.; Thakur, A.; Kumar, P. Green synthesis of glowing carbon dots from Carica papaya waste pulp and their application as a label-freechemo probe for chromium detection in water. *Sens. Actuators B Chem.* **2019**, *283*, 363–372. [CrossRef]
48. Ávila, J.M.; Ayala, M.R.; Kumar, Y.; Pérez-Tijerina, E.; Robles, M.A.; Agarwal, V. Avocado seeds derived carbon dots for highly sensitive Cu (II)/Cr (VI) detection and copper (II) removal via flocculation. *Chem. Eng. J.* **2022**, *446*, 137171. [CrossRef]
49. Liu, C.; Zhang, F.; Hu, J.; Gao, W.; Zhang, M. A Mini Review on pH-Sensitive Photoluminescence in Carbon Nanodots. *Front. Chem.* **2021**, *8*, 605028. [CrossRef]
50. Wang, H.; Liu, S.; Xie, Y.; Bi, J.; Li, Y.; Song, Y.; Cheng, S.; Li, D.; Tan, M. Facile one-step synthesis of highly luminescent N-doped carbon dots as an efficient fluorescent probe for chromium(vi) detection based on the inner filter effect. *New J. Chem.* **2018**, *42*, 3729–3735. [CrossRef]
51. Ma, Y.; Chen, Y.; Liu, J.; Han, Y.; Ma, S.; Chen, X. Ratiometric fluorescent detection of chromium(VI) in real samples based on dual emissive carbon dots. *Talanta* **2018**, *185*, 249–257. [CrossRef]
52. Huang, S.; Yang, E.; Yao, J.; Chu, X.; Liu, Y.; Xiao, Q. Nitrogen, phosphorus and sulfur tri-doped carbon dots are specific and sensitive fluorescent probes for determination of chromium(VI) in water samples and in living cells. *Microchim. Acta* **2019**, *186*, 851. [CrossRef]
53. Xiao, N.; Liu, S.G.; Mo, S.; Li, N.; Ju, Y.J.; Ling, Y.; Li, N.B.; Luo, H.Q. Highly selective detection of p-nitrophenol using fluorescence assay based on boron, nitrogen co-doped carbon dots. *Talanta* **2018**, *184*, 184–192. [CrossRef]
54. Qin, K.; Zhang, D.; Ding, Y.; Zheng, X.; Xiang, Y.; Hua, J.; Zhang, Q.; Ji, X.; Li, B.; Wei, Y. Applications of hydrothermal synthesis of *Escherichia coli* derived carbon dots in in vitro and in vivo imaging and *p*-nitrophenol detection. *Analyst* **2020**, *145*, 177–183. [CrossRef] [PubMed]
55. Tummala, S.; Lee, C.-H.; Ho, Y.-P. Boron, and nitrogen co-doped carbon dots as a multiplexing probe for sensing of p-nitrophenol, Fe (III), and temperature. *Nanotechnology* **2021**, *32*, 265502. [CrossRef] [PubMed]
56. Wang, X.; Liu, Y.; Wang, Q.; Bu, T.; Sun, X.; Jia, P.; Wang, L. Nitrogen, silicon co-doped carbon dots as the fluorescence nanoprobe for trace p-nitrophenol detection based on inner filter effect. *Spectrochim. Acta Part A Mol. Biomol. Spectrosc.* **2021**, *244*, 118876. [CrossRef] [PubMed]
57. El-Shaheny, R.; Yoshida, S.; Fuchigami, T. Graphene quantum dots as a nanoprobe for analysis of o- and p-nitrophenols in environmental water adopting conventional fluorometry and smartphone image processing-assisted paper-based analytical device. In-depth study of sensing mechanisms. *Microchem. J.* **2020**, *158*, 105241. [CrossRef]
58. Bhati, A.; Anand, S.R.; Saini, D.; Sonkar, S.K. Sunlight-induced photoreduction of Cr(VI) to Cr(III) in wastewater by nitrogen-phosphorus-doped carbon dots. *Npj Clean Water* **2019**, *2*, 12. [CrossRef]
59. Bogireddy, N.K.R.; Mejia, Y.R.; Aminabhavi, T.M.; Barba, V.; Becerra, R.H.; Flores, A.D.A.; Agarwal, V. The identification of byproducts from the catalytic reduction reaction of 4-nitrophenol to 4-aminophenol: A systematic spectroscopic study. *J. Environ. Manag.* **2022**, *316*, 115292. [CrossRef]
60. Strachan, J.; Barnett, C.; Masters, A.F.; Maschmeyer, T. 4-Nitrophenol Reduction: Probing the Putative Mechanism of the Model Reaction. *ACS Catal.* **2020**, *10*, 5516–5521. [CrossRef]